J Mater Sci (2010) 45:1299–1306
DOI 10.1007/s10853-009-4082-7

Solvent control of cellulose acetate nanofibre felt structure produced by electrospinning

Daniel Haas · Stefan Heinrich · Peter Greil

Received: 28 August 2009 / Accepted: 24 November 2009 / Published online: 5 December 2009

Abstract Non-woven structures of cellulose acetate (CA) fibres of 90 nm–5 μm in diameter (spinning parameters 90 nm beaded fibres: 12% CA in EtOH-DMSO 1/1, 22 kV, 30 cm, 0.5 mL/h; maximum 5 μm diameter fused fibres spun with 14% CA in Ac-BenzOH 2/1, 22 kV, 24 cm, 13 mL/h) were produced by electrospinning. On the basis of Hansen solubility theory, composition of binary solvent mixtures (ketones—acetone, methyl ethyl ketone (MEK), and alcohols—benzyl alcohol, propylene glycol and dimethylsulphoxide) was optimized with respect to control of fibre felt morphology. Fibre networks of high packing density were obtained with binary low-volatile alcohols/MEK solvent mixtures, a decreased spinning distance and an increased feed rate. Substituting MEK by acetone in the solvent mixture resulted in the formation of nanofibre felt with a low degree of fibre cross-links. Thus, solvent control is a key aspect for control of electrospun fibre felt structures, which may serve as scaffolds for tissue engineering.

Introduction

Electrospinning is a technique that can be used to produce nanofibres from a polymeric solution or melt under the influence of a high electrostatic field. The polymeric solution is initially ejected from the tip of a fine orifice or spinneret maintained at a potential up to several tens of kilovolts by a DC power supply [1–3]. The electrostatic repelling force of the charges deforms the pendant drop into a conical shape (Taylor Cone). If the potential is further increased, the electrostatic force overcomes the surface tension force of a polymer solution and drags the polymer to form fibre streams. The fibre streams will become unstable to a whip-like motion that further elongates them and reduces their diameter [4, 5]. Solvent evaporates in the process, and dry fibres are collected on the collector plate as a non-woven mat. The diameter of the fibres obtained in the electrospinning process ranges from 10 μm down to 10 nm, which is nearly two to three orders less than that obtained by conventional polymer melt or solution spinning process [1–3].

Highly porous nanofibre felts electrospun from natural or synthetic biodegradable polymers have drawn increased interest for use as scaffolds for tissue engineering in regenerative medicine. Electrospun non-woven webs composed of sub-micron diameter fibres may serve as functional substrates to grow soft tissues for cartilage and skin repair. Non-woven structures of nanofibres provide a highly accessible three-dimensional structure characterized by a high surface area-to-volume ratio and three-dimensional interconnected pore network, both of which enhance cell attachment and proliferation [6]. Furthermore, cells attach and organize well around fibres with diameters smaller than the diameter of the cells [7]. Fibroblasts showed significantly higher proliferation on fibre matrices with a diameter in the range 350–1100 nm [8]. Electrospinning of biopolymeric nanofibre scaffolds, however, often involves aggressive and toxic solvents to achieve optimized fibre formation conditions [9]. Furthermore, electrospun non-woven mats may exhibit quite a poor tensile strength and a low Young's modulus because the loosely packed fibres without extended cross-linking are not able to transfer normal and shear stress upon mechanical loading effectively [10, 11]. The mechanical properties of non-woven fibre felts were improved by alignment of the fibres which

D. Haas (✉) · S. Heinrich · P. Greil
Department of Materials Science (Glass and Ceramics), University of Erlangen-Nuremberg, Erlangen, Germany
e-mail: daniel.haas@ww.uni-erlangen.de

was achieved by spinning on modified collector types [12–15], modification of the spinning process parameters, or postprocessing, respectively.

A high number of solid fibre cross-links per fibre length was found to be a key factor to create a high stiffness and loading capacity of highly porous fibre felts [16]. In this study, cellulose acetate (CA) was chosen to serve as a model system for developing felts of various cross-linking and fibre packing structure. Acetone and dimethylacetamide (DMA) at a ratio of 2:1 was found to dissolve CA in a range from 12.5 to 20 wt% and to allow continuous electrospinning of CA fibres. Lower amounts of DMA as cosolvent (extreme case: pure acetone) resulted in clogging of the nozzle because of the too high volatility [17]. Another possibility is the addition of water as cosolvent at 10–15 wt% to acetone [18]. A mixed solvent of chloroform/methanol was also shown to produce thin beaded CA fibres [19]. Even ternary mixtures of acetone, dimethylformamide (DMF) and trifluoroethylene were reported as solvent for CA [16]. However, search for suitable solvents was either based on trail and error, experiences from similar polymer systems or solubility models limited by physico-chemical database [17, 18, 20]. The focus of our study was directed on the role of solvent volatility behaviour for controlling the felt structure with particular emphasis on fusion at the fibre overlying points and packing density. Hansen's theory of solubility was applied to select non-toxic binary solvent systems optimized for manufacturing of electrospun fibre networks with adjustable degree of fibre fusion.

Experimental procedure

Solvent selection

Cellulose acetate (Aldrich, 180955) with a molecular weight of 30,000 g/mol and an acetyl content of 39.8 wt% was dissolved in a mixture of various solvents: Methylethylketone (MEK, Carl Roth, 8403.2), Acetone (Ac, Merck, 20063.467), Benzyl alcohol (Carl Roth, 0336.2), 1,2-Propanediol (Carl Roth, 0340.21), Ethyl alcohol (VWR 20821.321) and Dimethylsulphoxide (DMSO, Fluka, 41640). All the chemicals were used as received. On the basis of the solubility ranges derived from calculations with the particular Hansen parameters [21], a set of five spinning solutions (Table 1a–e) with different solvent compositions was prepared by mixing in a screw top jar. Clear solutions were obtained after 24 h. The concentration of CA was kept constant at 14 wt% except for acetone/DMSO mixture (18 wt%, spinning dope "c"). For ethanol/DMSO mixture, concentration was varied between 8 and 24 wt% (spinning dope "d", Table 1).

Appropriate solvent compositions were selected from evaluation of the solubility behaviour following Hansen′s theory of solubility [21]. The solubility parameter ∂ (named Hildebrand parameter) is a numerical value that specifies the relative solvency behaviour of a specific solvent

$$\partial = \sqrt{E_{\mathrm{d}}} = \left(\frac{\Delta H - RT}{V_{\mathrm{m}}}\right)^{1/2} \quad (1)$$

where E_{d} is the cohesive energy density, ΔH is the heat of vaporization, R is the gas constant, T is the temperature and V_{m} is the molar volume. Hansen found that ∂ may be separated into contributions of fundamental molecular interactions

$$\partial = \sqrt{\partial_d^2 + \partial_p^2 + \partial_h^2} \quad (2)$$

where ∂_{d}, ∂_{p} and ∂_{h} represent the dispersion force, the polar force, and the hydrogen bonding force, respectively, and are called Hansen parameters [21]. The SI unit of all solubility parameters is $\mathrm{MPa}^{1/2}$ (formerly $\mathrm{cal}^{1/2}\,\mathrm{cm}^{-3/2}$). Values of ∂_{d}, ∂_{p} and ∂_{h} at room temperature for a variety of solvents for CA are presented in Table 2. According to Hansen, an approximately spherical area of solubility may be constructed in a three-dimensional coordinate system of ∂_{d}, ∂_{p} and ∂_{h}. The radius of that sphere (7.6 $\mathrm{MPa}^{1/2}$ for cellulose acetate, [21]) is called interaction radius r

$$r = \left[4\left(\partial_{\mathrm{d}} - \partial_{\mathrm{d,CA}}\right)^2 + \left(\partial_{\mathrm{p}} - \partial_{\mathrm{p,CA}}\right)^2 + \left(\partial_{\mathrm{h}} - \partial_{\mathrm{h,CA}}\right)^2\right]^{1/2} \quad (3)$$

$\partial_{\mathrm{d,CA}}$, $\partial_{\mathrm{p,CA}}$ and $\partial_{\mathrm{h,CA}}$ represent the coordinates of the centre of the Hansen sphere and are given by the Hansen parameters of the polymer, in this case CA, Fig. 1a. Every solvent S or solvent mixture whose fundamental molecular

Table 1 Composition of spinning dopes and particular spinning parameters

#	Solvent system	Ratio	CA-conc. (wt%)	Distance (cm)	Voltage (kV)	Feed rate (mL/h)
(a)	Ac/BenzOH	2/1	14	24	22	13
(b)	MEK/BenzOH	4/1	14	30	22	13
(c)	Ac/DMSO	2/1	18	30	22	0.5
(d)	EtOH/DMSO	1/1	var. 8…24	30	22	0.5
(e)	Ac/BenzOH	2/1	14	33	22	2.6

Table 2 Solubility parameters of various solvents and cellulose acetate [19]

Liquid	Solubility parameter ($MPa^{1/2}$)				d^*
	∂	∂_d	∂_p	∂_h	
Acetone (Ac)	20.00	15.50	10.40	7.00	−0.13
Methyl ethyl ketone (MEK)	19.00	16.00	9.00	5.10	−1.09
Propylene glycol ($Pr(OH)_2$)	30.20	16.80	9.40	23.30	−5.63
Chloroform	19.00	17.80	3.10	5.70	−3.5
Dimethylacetamide	22.70	16.80	11.50	10.20	3.7
Dimethylformamide	24.80	17.40	13.70	11.30	5.0
Dimethylsulphoxide (DMSO)	26.70	18.40	16.40	10.20	3.8
Ethanol	26.50	15.80	8.80	19.40	−3.2
Methanol	29.60	15.10	12.30	22.30	−5.7
Benzyl alcohol (BeOH)	23.80	18.40	6.30	13.70	0.6
Water	47.80	15.60	16.00	42.30	−24.4
Cellulose acetate	25.06	18.60	12.70	11.00	(7.6)

interaction parameters ($\partial_{d,s}$, $\partial_{p,s}$ and $\partial_{h,s}$) are located within the Hansen sphere should be able to dissolve CA readily, whereas those located outside are unlikely of dissolving CA, Fig. 1b.

The parameter d^* representing the distance between the solvent coordinates and the surface of the Hansen sphere, Fig. 1a, can be calculated by

$$d* = r - d = r - \left[4\left(\partial_{d,s} - \partial_{d,CA}\right)^2 + \left(\partial_{p,s} - \partial_{p,CA}\right)^2 + \left(\partial_{h,s} - \partial_{h,CA}\right)^2\right]^{1/2} \quad (4)$$

where d is the distance between the solvent coordinates and the polymer coordinates. A solvent lying outside the solubility sphere, i.e. $d^* < 0$, may be combined with another solvent to a binary mixture A–B. For a specific composition of the binary mixture A–B with the solubility parameter located inside the sphere, i.e. $d^* > 0$, solution of CA can be expected, Fig. 1b.

The solubility parameter ∂_{A-B} of binary solvent mixture of two solvents A and B is given by the volume fractions v_i of each solvent and the equivalent Hansen Parameters ∂_i of A and B.

$$\partial_{A-B} = \sum \partial_i v_i \quad (5)$$

On the basis of the solubility criteria a set of solvents and binary solvent mixtures was selected for the electrospinning experiments, Table 1.

Electrospinning

Nanofibre non-woven felts were produced by electrospinning of CA solution at room temperature. The rheological behaviour of the spinning dopes was analysed with a rotational viscosimeter (Physica UDS 200, Paar Physica, Stuttgart, Germany) in cone plate arrangement (cone diameter 50 mm, cone angle 2°) at 20 °C and under solvent saturated atmosphere. In the electrospinning setup, a 5-mL syringe was positioned vertically above the collector. The needle diameter was 800 µm. An electrical potential difference between needle and collector plate was applied (IT 30, Miles HiVolt Ltd., England). For spinning of non-uniform structures with a lateral gradient in thickness and porosity, a static circular colletor (diameter 180 mm) was used, Fig. 2a. In order to obtain felt deposit of uniform thickness, the syringe was positioned with an excentrical distance of 60 mm from the rotating axis, Fig. 2b. The turning collector (diameter 200 mm) was rotated with 1 rps. The polymer solution was fed by means of a modified micropump (Perfusor® Secura FT, B. Braun Melsungen

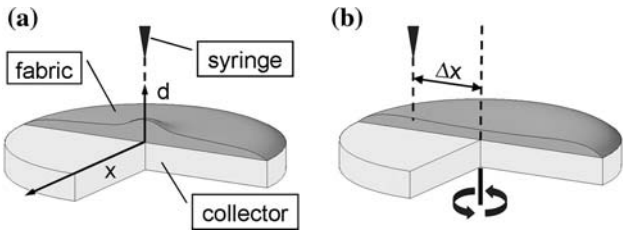

Fig. 2 Arrangement of syringe and collector: **a** centrical syringe, static collector; **b** excentrical syringe, turning collector

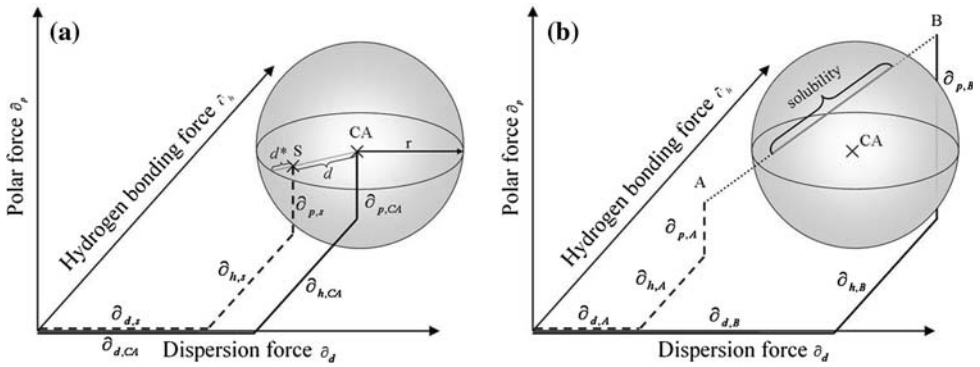

Fig. 1 Schemes of a Hansen diagram: **a** d^*-calculation for a single solvent; **b** solubility range for a mixture of solvent A and solvent B

AG, Germany). The fibre felt was collected on a 13-μm thick aluminium foil covered metal plate collector positioned at a distance of 24, 30 or 33 cm from the tip of the syringe, respectively. Electrospinning of the CA solution was conducted by varying the voltage (19 and 22 kV), the flow rate of the solution (0.5, 2.6 and 13 mL/h), and the solvent composition. Whilst a DMSO/ethyl alcohol mixture was spun at different concentrations ranging from 8 to 24 wt%, the concentration was kept constant at 14 and 18 wt%, respectively, for the other spinning dopes (Table 1).

Fibre and fibre felt microstructure

The morphology and the diameter of the collected fibres were analysed by scanning electron microscopy (SEM, FEI, Quanta 200, Eindhoven, Netherlands). Porosity P of the fibre structures was calculated by

$$P = 1 - \frac{\rho_{\text{geo}}}{\rho_{\text{CA}}} \tag{6}$$

with ρ_{geo} the geometric bulk density of the felt i.e. deposit weight to volume and ρ_{CA} the density of the CA fibre (1.3 g/cm^3). The thickness was measured tactilely with a dial indicator (1 μm resolution, flat contact point, diameter 10 mm). The area was measured by optical scanning with 600 dpi resolution and subsequent image analysis (ImageJ V. 1.38 Wayne Rasband, National Institutes of Health, Bethesda/MD USA). In order to evaluate the degree of fibre fusion of the fibre network, the fibre diameter and the distance of the fibre connections from crossing point to crossing point were measured on SEM images. Mean values were derived from at least 50 fibres.

Results and discussion

Cellulose acetate spinning solution

The composition of the binary solvent mixtures strongly influences dissolution behaviour and viscosity of the resulting spinning solution [22]. Figure 3 shows the solubility tendency for binary solvent systems expressed as the distance d^* as a function of composition. Positive values of d^* indicate solubility capability, whereas negative values of d^* represent compositions not able to dissolve CA.

Ac/DMA solvent mixture shows a continuously increasing d^* with DMA fraction. An even superior dissolving power is expected for an acetone/DMSO mixture compared to acetone/DMA. Benzyl alcohol added to acetone promotes a solubility over the whole range of mixture but has a lower dissolving power for high concentrations compared to the DMSO-based solvents. An ethanol/DMSO mixture shows the highest dissolving power but a reduced

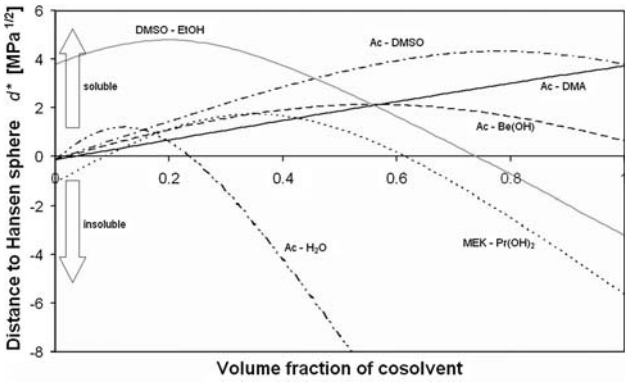

Fig. 3 Solubility range of CA for various solvents derived from Hansen solubility parameters

range of solvent composition. The strongest dissolving power expected from the evaluation of solubility parameters is attributed to a solvent mixture with its coordinates located in the Hansen diagram close to the one from CA i.e. with maximum value of d^*. A DMSO/benzyl alcohol mixture of 65 to 35 (v/v) reaches a d^*-value of 7 MPa$^{1/2}$ which is higher than all single solvents considered in this study.

Solubility of the polymer, however, is a necessary but not sufficient condition for spinnability. The jet of the spinning dope is stretched into a fibre shape and this shape has to be stabilized before reaching the collector. Insufficient stabilization, however, may cause fragmentation due to Rayleigh-instability, which results in the formation of droplets instead of a fibre and electrospraying is likely to occur [23]. Stabilization of the fibre will be facilitated when the spinning dope exhibits a high initial viscosity and/or a rapid increase of the viscosity due to accelerated evaporation of the solvent during fibre formation. For that reason, the information about solubility range of a mixed solvent is even more important than the maximum solubility. Since in a binary solvent mixture evaporation of the component with higher volatility is likely to occur, both the viscosity as well as the dissolution capability of the solvent system may change significantly. Analysis of the rheological behaviour indicated that for low viscosity at low polymer concentrations, electrospraying occurs [23, 24]. At higher viscosity, periodical beads on string are formed. Further increase of viscosity leads to smooth fibres [3, 20].

Figure 4 shows the dependence of zero shear viscosity of a binary ethanol/DMSO solvent (1:1 by weight, which proved to be a good compromise between solubility and evaporation rate) on CA concentration and SEM micrographs of selected fibre structures. Three different regimes can be expected with respect to the composition dependence of viscosity. The increase of the viscosity can be fitted with a power law dependence for each concentration regime [25].

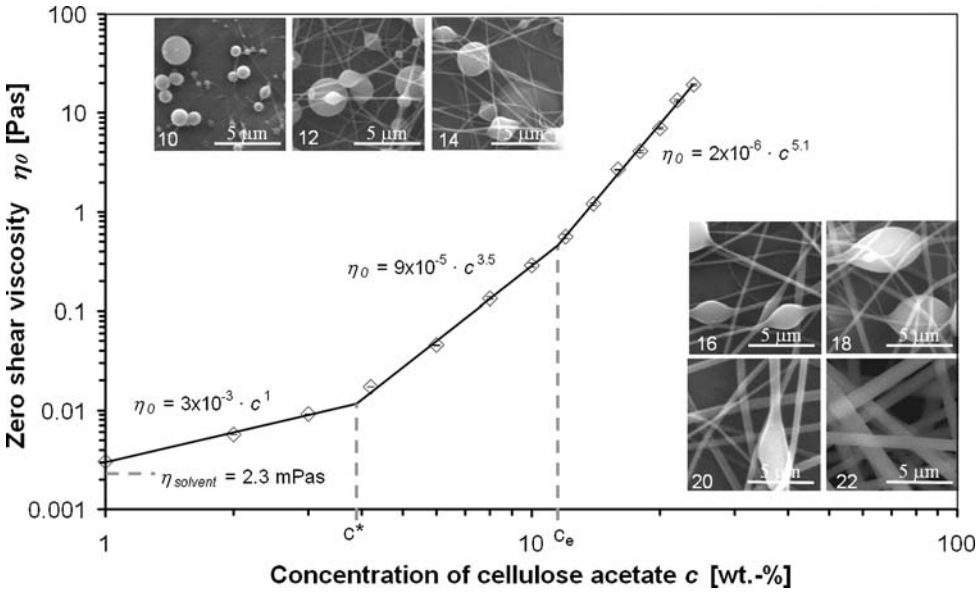

Fig. 4 Dependence of zero shear viscosity on cellulose acetate concentration and corresponding fibre images

$$\eta \propto c^n \tag{7}$$

For low concentrations (diluted regime), the interaction between separated polymer chains is low and an exponent $n \approx 1$ is predicted. Above a critical polymer concentration c^*, the polymer chains can overlap, but do not entangle each other (semidilute unentangled regime, $n = 1.25$). At high concentration above c_e, overlapping of the polymer chains favours entanglement which gives rise for a much stronger interaction (semidilute entangled regime, $n = 4.8$). For CA (molecular weight of 30,000 g/mol), the boundary concentrations were found at $c* \approx 4$ wt% and $c_e \approx 12$ wt%. The differences in molecular interaction and hence in the viscosity of the spinning dope have a strong impact on the fibre morphology produced as confirmed by SEM analysis, Fig. 4. Individual spherical beads are observed for concentrations lower than 12 wt% (electrospraying regime, $n = 3.5$). Fibres can only be spun for concentrations exceeding 12 wt%. With increasing viscosity of the spinning dope, the bead shape changes gradually from spherical to elongated ellipsoidal beads ($n = 5.1$). Finally, smooth fibres with no periodical thickness variations were obtained at concentrations higher than 20 wt%, Fig. 4 [19, 24, 26].

The molecular structure of the dissolved polymer (cellulose acetate) also affects solution viscosity. Whilst a branched molecular structure tends to reduce/hinder the chain interaction (n decreases) hydrogen bonding may intensify chain interaction (n increases) which also applies for CA [24, 27, 28]. In all the cases, the entanglement concentration c_e was the minimum concentration where beaded fibres could be obtained in coincidence with our results [28]. The concentration needed for smooth fibres was 1.7 times c_e for CA compared to 2–2.5 times c_e for PET copolymers [27].

The mean diameter of the fibres d_F increased with the zero shear viscosity following a power law dependence

$$d_F \propto \eta_0^m \tag{8}$$

Simulations based on allometric scaling laws predicted an exponent m of 0.5 [29], whilst experimental results showed exponents between 0.5 and 0.8 [24, 27, 30]. Spinning experiments for CA dissolved in ethanol/DMSO revealed an exponent of 0.71, Fig. 5.

The flight path of an electrified liquid was simulated by localized induction approximation [31]. Whilst for the case of constant viscosity, the radius of the envelope cone was predicted to increase abruptly due to bending instability it should grow evenly if the viscosity increases. High-speed camera observations of the spinning process proved the convolute path with evenly increasing radius but constant drift velocity in spinning direction caused by the viscosity increase during spinning [32]. It was demonstrated that even low concentrations of a polymer can be spun if the jet

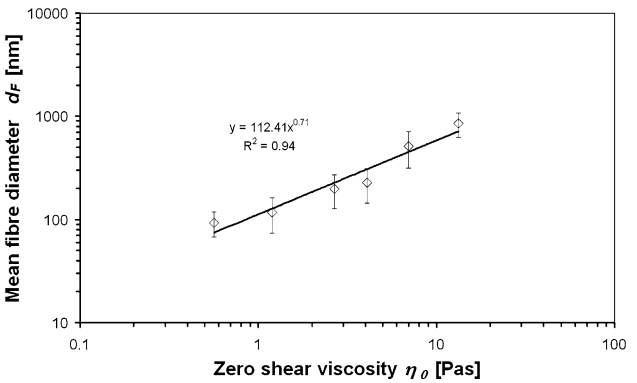

Fig. 5 Dependence of zero shear viscosity on resulting fibre diameter

is stabilized by accelerated evaporation of the solvent [19, 33]. Our results on DMSO-based binary solvent mixtures reveal that the transition from spraying to spinning (12 wt%) is shifted to lower concentrations (8–10 wt%) if ethanol is replaced by acetone which exhibits a higher volatility than ethanol.

Binary DMSO/acetone system was the solvent mixture providing the largest processing window concerning mixing ratio and volume flow rate of the spinning dopes. Acetone/ethanol system shows a good spinnability, but volatility of ethanol is too low to achieve smooth fibre spinning at low concentrations and beads are formed instead.

Fibre felt structure

Depending on the spinning dope composition and the process conditions, diameters of the fibres varied from 90 nm to 5 μm and the fibre felt structure showed porosities between 60 and 97%. Figure 6 shows SEM micrographs of characteristic felt structures obtained from electrospinning of acetone/benzyl alcohol, MEK/benzyl alcohol and acetone/DMSO system, respectively (Fig. 6a corresponds to spinning dope "a", Table 1). The morphology characteristics of the electrospun fibre networks are summerized in Table 3.

Cellulose acetate fibres from acetone/benzyl alcohol solvent system form highly intereconnected felt-like structures with a high packing density and a low porosity, Fig. 6a. Replacing acetone by MEK with an even lower volatility finally resulted in similar structures. If the fraction of the volatile component MEK is increased from 2/1 to 4/1 whilst keeping the other parameters constant, the resulting felt consists of smooth fibres with a diameter ranging from 1 to 3 μm, which are barely welded at the cross-over points, Fig. 6b. This is typical if the spinning dope stays in a gel-like condition which is the case for solvents with a low vapour pressure. Similar results were reported for the spinning of gelatin fibres with cosolvents of low vapour pressure and high boiling point [34]. A decrease of the feed rate leads to sub-μm fibres, approving the well-known coherency of decreasing feed rate and decreasing fibre diameter [35]. Figure 6c shows fibres spun from an acetone/DMSO system. The resulting felt is free of defects but the fibres do not form interconnected structures as indicated by the absence of solid cross-links.

Characterization of electrospun fibre felt microstructure is a key aspect for optimization of processing parameters with respect to tailoring of mechanical properties as well as permeability of porous fibre felt materials. Soldering of the fibres at the fibre overlying points produces a fibre network structure with a high and continuous porosity. In this study,

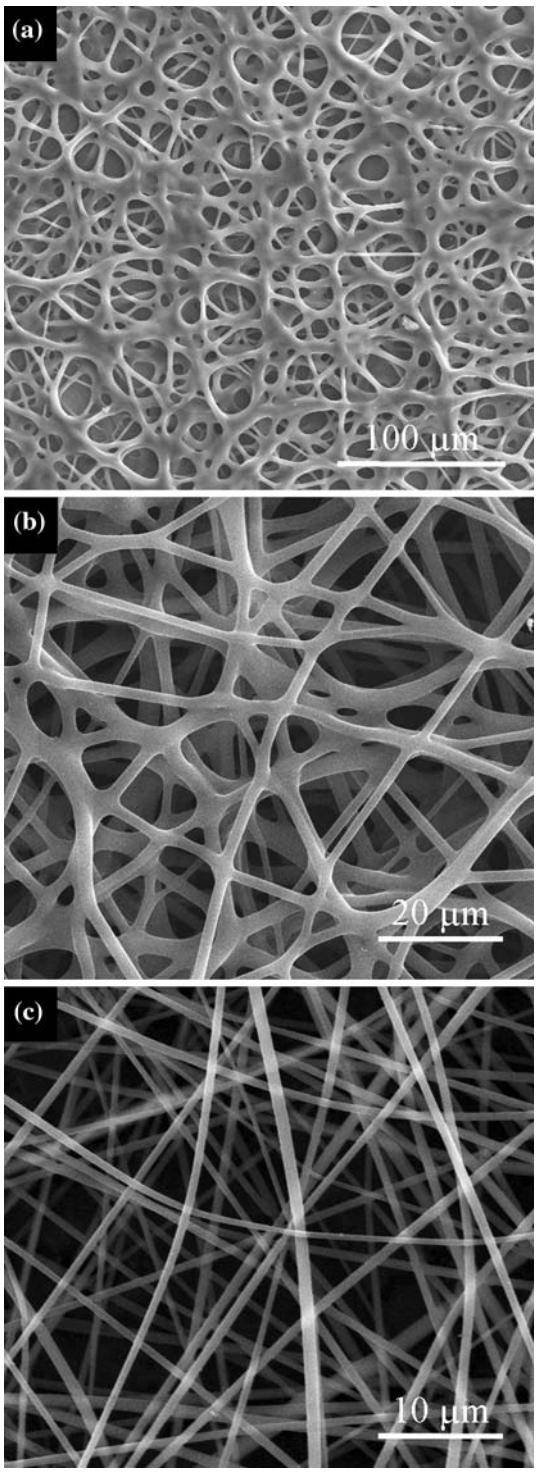

Fig. 6 Non-wovens spun from different spinning dopes and various spinning conditions (details see Table 1)

fibre cross-linking and porosity was characterized by means of a simplified geometrical model of a representative unit cell analogon. Since the fibre felt formation process during electrospinning can be considered as a layerwise deposition of fibre material on the collector

Table 3 Morphology characteristics of electrospun fibre networks

#	Solvent system	Ratio	Fibre thickness t_F (μm)	Porosity P (%)	Cross-link distance l (μm)	Interpenetration ζ
(a)	Ac/BenzOH	2/1	3.41 ± 1.78	66	8.42 ± 3.95	0.33
(b)	MEK/BenzOH	4/1	2.03 ± 0.66	80	8.63 ± 5.48	0.25
(c)	Ac/DMSO	2/1	0.65 ± 0.13	92	4.67 ± 2.91	−0.19

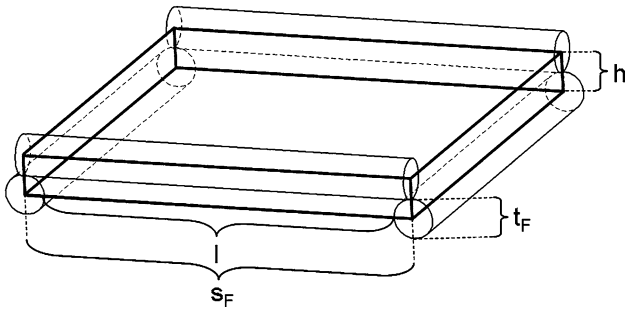

Fig. 7 Unit cell model for fibre networks

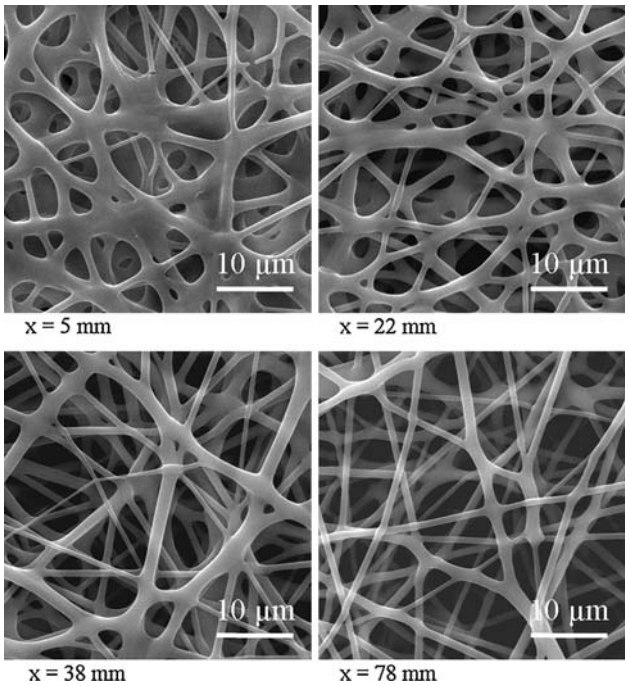

Fig. 8 Electrospun gradient fibre structures with different degrees of cross-linking and distance from collector centre x

substrate, structure characterization is focussed on deposition of geometrical fibre arrangement in a deposit layer. Figure 7 shows an idealized unit cell. Four fibre segments of length s_F and fibre thickness t_F form a rectangular cell of a volume $s_F^2 \cdot h$ where h is the cell height. For the case of the fibre segments do not penetrate i.e. no solid cross-link is formed h equals to the fibre thickness t_F and the porosity of the unit cell P can be derived from

$$P = 1 - \frac{\frac{t_F^2}{4}\pi \cdot s_F}{s_F^2 \cdot h} = 1 - \frac{t_F^2 \cdot \pi}{4 s_F \cdot h} \tag{9}$$

The fibre thickness t_F and the mean free length of the fibres between the crossing points l can be measured from SEM micrographs. If the fibres are fused at the cross-links, then $h < t_F$.

$$h = \frac{t_F^2 \pi}{4 s_F \cdot (1 - P)} = \frac{t_F^2 \pi}{4 \cdot (l + t_F) \cdot (1 - P)} \tag{10}$$

If P is set equal to the total felt porosity, an average height of the unit cell can be calculated from Eq. 10. The degree of interpenetration ζ is given by the ratio of unit cell height and fibre diameter.

$$\zeta = 1 - \frac{h}{t_F} = 1 - \frac{t_F \cdot \pi}{4 \cdot (l + t_F) \cdot (1 - P)} \tag{11}$$

ζ may vary from 0 to 1 and represents a degree of fibre interpenetration when forming a cross-link. Negative values of ζ are expected for fibres that do not even touch each other but have some space in between. The resulting degrees of interpenetration are summarized in Table 3 for the fibre networks spun from different solvent systems, Fig. 6. Whilst Fig. 6a and b shows highly interconnected structures with degrees of interpenetration of 0.33 and 0.25, respectively, the felt structure given in Fig. 6c has a negative degree of interpenetration. Same analysis was also done for the gradient structure spun on a static collector, Figs. 2a and 8. The degree of interpenetration ranges from 0.06 close to the edge of the collector to 0.49 at the centre right beyond the needle Table 4.

Thermal post-treatment of thermoplastic materials was demonstrated to create connection points between the fibres, which improved the mechanical properties of the porous fibre network significantly [16, 36]. Thus, control of the solvent properties in a mixed solvent may well be used to generate highly interconnected fibre felt structures. These porous structures combine a high open cell porosity with a high density of solid fibre cross-links, which offers improved mechanical properties as resistance against shear, compressive and tensile loading stresses.

Conclusions

Hansen solubility theory was applied to select non-toxic solvent compositions of ketones and alcohols/DMSO

Table 4 Morphology characteristics of electrospun gradient structures as a function of the distance to the collector centre

Distance x (cm)	0.5	2.2	3.8	7.8
Porosity P (%)	60	66	80	86
Cross-link distance l (μm)	3.7 ± 3.3	3.0 ± 1.7	4.3 ± 2.1	4.9 ± 2.4
Fibre thickness t_F (μm)	1.3 ± 0.74	1.0 ± 0.39	1.0 ± 0.35	1.0 ± 0.35
Touching Porosity P_T (%)	80	80	85	87
Interpenetration ζ	0.49	0.40	0.23	0.06

suitable for electrospinning of CA solutions. Fibre felts with different degrees of fibre cross-linking were produced by varying the solvent volatility and the spinning parameters. Characterization of the fibre felts was done by SEM analysis, and the cross-linking density was verified by means of a geometrical model correlating cross-linking density and porosity. Highly connected fibre networks with a porosity of 60–85% containing a high number of solid cross-links offer a high potential to serve as scaffold structures in tissue engineering.

Acknowledgements Special thanks go to Dr. Jochen Kaschta from the chair of polymer materials for helpful discussions. Financial support from German Science Foundation (DFG) under contract number GR 961/26-1 is gratefully acknowledged.

References

1. Subbiah T, Bhat GS, Tock RW, Pararneswaran S, Ramkumar SS (2005) J Appl Polym Sci 96:557
2. Li D, Xia YN (2004) Adv Mater 16:1151
3. Huang Z-M, Zhang Y-Z, Kotaki M, Ramakrishna S (2003) Compos Sci Technol 63:2223
4. Reneker DH, Yarin AL, Fong H, Koombhongse S (2000) J Appl Phys 87:4531
5. Shin YM, Hohman MM, Brenner MP, Rutledge GC (2001) Appl Phys Lett 78:1149
6. Yoshimoto H, Shin YM, Terai H, Vacanti JP (2003) Biomaterials 24:2077
7. Laurencin CT, Ambrosio AMA, Borden MD, Cooper JA (1999) Ann Rev Biomed Eng 1:19
8. Kumbar SG, Nukavarapu SP, James R, Nair LS, Laurencin CT (2008) Biomaterials 29:4100
9. Schiffman JD, Schauer CL (2008) Polym Rev 48:317
10. Liu HQ, Tang CY (2007) Polym J 39:65
11. Carrizales C, Pelfrey S, Rincon R, Eubanks TM, Kuang A, McClure MJ, Bowlin GL, Macossay J (2008) Polym Adv Technol 19:124
12. Inai R, Kotaki M, Ramakrishna S (2005) Nanotechnology 16:208
13. Courtney T, Sacks MS, Stankus J, Guan J, Wagner WR (2006) Biomaterials 27:3631
14. Teo WE, Ramakrishna S (2006) Nanotechnology 17:R89
15. Greiner A, Wendorff JH (2007) Angew Chem Int Ed 46:5670
16. Ma ML, Hill RM, Lowery JL, Fridrikh SV, Rutledge GC (2005) Langmuir 21:5549
17. Liu H, Hsieh Y-L (2002) J Polym Sci Part B: Polym Phys 40:2119
18. Son WK, Youk JH, Lee TS, Park WH (2004) J Polym Sci Part B: Polym Phys 42:5
19. Tungprapa S, Puangparn T, Weerasombut M, Jangchud I, Fakum P, Semongkhol S, Meechaisue C, Supaphol P (2007) Cellulose 14:563
20. Jarusuwannapoom T, Hongrojjanawiwat W, Jitjaicham S, Wannatong L, Nithitanakul M, Pattamaprom C, Koombhongse P, Rangkupan R, Supaphol P (2005) Eur Pol J 41:409
21. Barton AFM (1985) Handbook of solubility parameters and other cohesion parameters. CRC Press Inc., Boca Raton, FL
22. Hoernschemeyer D (1974) J Appl Polym Sci 18:61
23. Shenoy SL, Bates WD, Frisch HL, Wnek GE (2005) Polymer 46:3372
24. Gupta P, Elkins C, Long TE, Wilkes GL (2005) Polymer 46:4799
25. Colby RH, Rubinstein M, Daoud M (1994) J Phys II 4:1299
26. Fong H, Chun I, Reneker DH (1999) Polymer 40:4585
27. McKee MG, Wilkes GL, Colby RH, Long TE (2004) Macromolecules 37:1760
28. McKee MG, Elkins CL, Long TE (2004) Polymer 45:8705
29. He JH, Wan YQ, Yu MY (2004) Int J Nonlin Sci Num 5:243
30. Baumgarten PK (1971) J Colloid Interf Sci 36:71
31. Yarin AL, Koombhongse S, Reneker DH (2001) J Appl Phys 89:3018
32. Reneker DH, Fong H (2005) Polymeric nanofibers. American Chemical Society, Washington, DC
33. Eda E, Shivkumar S (2007) J Appl Polym Sci 106:475
34. Choktaweesap N, Arayanarakul K, Aht-ong D, Meechaisue C, Supaphol P (2007) Polym J 39:622
35. Tan SH, Inai R, Kotaki M, Ramakrishna S (2005) Polymer 46:6128
36. Lee SJ, Oh SH, Liu J, Soker S, Atala A, Yoo JJ (2008) Biomaterials 29:1422